World Journal of Engineering Research and Technology
WJERT
www.wjert.org
SJIF Impact Factor: 7.029

NUMERICAL SIMULATION OF STEADY FLOW IN A PUMP AS TURBINE UNDER TYPICAL WORKING CONDITIONS

Ji-Wei Shen*[1], Qing-Ming Jin[2], He-Chao Guo[1], Zhi-Yang Zhao[1], Bo Wang[1], Ke-Xin Xie[1]

[1]College of Mechanical Engineering, Quzhou University, Quzhou, 324000, China.
[2]Wenzhou Bingyuan Intelligent Technology Co., Ltd., Wenzhou 325800, China.

Article Received on 10/01/2025 **Article Revised on 30/01/2025** **Article Accepted on 19/02/2025**

***Corresponding Author**
Ji-Wei Shen
College of Mechanical Engineering, Quzhou University, Quzhou, 324000, China.

ABSTRACT

Pump as Turbine are widely applied in high-pressure liquid energy recovery processes due to their low acquisition cost, high energy recovery efficiency, and long service life. This paper conducts a numerical simulation of the turbine process for the single-stage centrifugal pump based on the STMPLEC algorithm. The preliminary analysis was conducted on the flow field inside the hydraulic turbine when the medium is clear water, under different inlet flow rates. The turbulence kinetic energy contour, vorticity contour, and pressure and velocity contour, as well as streamline and velocity vector plots for the blade unfolded diagram, were obtained. The results show that as the inlet flow rate increases, the turbulence kinetic energy and vorticity inside the pump as turbine significantly increase. However, the velocity and pressure around the blades gradually decrease, and vortices are generated at the blade outlet. As the curve extends from the center of the impeller to the volute, the pressure and velocity gradually increase, while the turbulence kinetic energy significantly increases with the inlet flow rate.

KEYWORDS: Single-stage centrifugal pump, numerical simulation, internal flow field.

1 INTRODUCTION

Pump as turbine is a device that reverses the pump's operation, allowing it to function as a hydraulic turbine for energy conversion. The working principle is that the motor, originally used to drive the pump shaft, no longer drives the shaft. Instead, high-pressure liquid enters

the pump from the outlet, flows through the impeller, causing the impeller to rotate in reverse. This converts the liquid's pressure energy and kinetic energy into mechanical energy, which is output through the pump shaft. In recent years, with the increased awareness of energy conservation and emission reduction at both the national level and among the public, the issue of energy waste in industrial development has gained widespread attention from all sectors of society. So far, the application history of the pump as turbine in China can be traced back to the 1980s. They are mainly used in industries such as petrochemicals, refining, and seawater desalination, including hydrogenation cracking units and large-scale ammonia synthesis units in petrochemical industries. Currently, using a centrifugal pump in reverse as a hydraulic turbine is a highly effective method for recovering and utilizing liquid pressure energy. In this regard, scholars both domestically and internationally have done a great deal of work and achieved significant results. Tao Wang found that the efficiency curve of the forward-curved impeller became much flatter, and compared to the backward-curved impeller, the maximum efficiency significantly increased.[1] Singh and Nestmann conducted experimental research focusing on the impact of blade height and the number of blades on the hydraulic performance of axial flow pumps in turbine operating mode.[2] Singh also found that, without changing the main parameters of the pump's reverse operation mode, measures such as increasing the impeller outlet and the tailwater pipe can improve the efficiency of the hydraulic turbine.[3] Jun-hu Yang studied the impact of different blade inlet angles and wrap angles on the optimal efficiency point of the hydraulic turbine.[5] Sun-Sheng Yang used full-flow field and structured grid techniques to perform numerical calculations of the internal flow in the hydraulic turbine scenario.[6] Fernandez used the sliding mesh technique to study the evolution characteristics of the external characteristics and internal flow field of the hydraulic turbine, focusing on the unsteady variation characteristics of the radial force acting on the impeller under reverse flow conditions.[7] Jose and Wang Chunlin used CFD technology to perform numerical simulations of the internal unsteady flow in a double-suction centrifugal pump under both forward and reverse operating modes, and compared the external characteristics with the internal flow.[8,9] Derakhshan conducted a detailed analysis of the internal flow structure of the hydraulic turbine through numerical simulation, and then compared the computational results with experimental data. He found that ignoring the fluid inside the front and rear chambers during the numerical calculation process led to a larger prediction error in the turbine's performance.[10] With the rapid development of computational fluid dynamics (CFD) and computer technology, numerical computation has become an important method for studying the internal flow characteristics of pumps and hydraulic

turbines. This study will use numerical simulation technology to analyze the internal flow field of a single-stage cantilever hydraulic turbine with a specific speed of 23.1 under different inlet flow rates. The aim is to initially understand the basic characteristics of the internal flow field variation in the pump-turbine.

2 Computational Model and Method

2.1 Computational Model: The main design parameters and dimensions of the pump as turbine are as follows: flow rate Q=12.5m^3/h, head H=80.78m, shaft power P=6.67kW, efficiency η=42.41%, rotational speed n=2900r/min, turbine impeller inlet diameter D_1=52mm, impeller outlet diameter D_2=242mm, impeller outer diameter D_3=242mm, impeller outlet width b_2=4mm, Blade outlet angle β_1=26°, volute base circle diameter D_4=248mm, Blade wrap angle β_2=155°.

2.2 Mesh Generation: ANSYS ICEM-CFD is powerful and professional pre-processing software widely used in the field of Computational Fluid Dynamics (CFD). It features advanced mesh generation capabilities, offering a wide range of mesh generation techniques, including structured meshes, unstructured meshes, and hybrid meshes. Depending on the different geometric shapes and computational requirements, the most suitable mesh type can be flexibly selected. For regions with regular shapes, structured meshes can be used, while unstructured meshes are more suitable for complex surfaces and boundaries. The total number of cells is 1,032,286. When creating the components, there are four main parts: the inlet extension section, impeller, volute, and tail water pipe. They are meshed as follows: hexahedral mesh, tetrahedral mesh, tetrahedral mesh, and hexahedral mesh, respectively. During the meshing process, we ensured that the mesh quality was above 0.2, and the computational domain for the pump as turbine is shown in Figure 1.

Figure 1: Computational Domain.

2.3 Control Equations: The numerical calculation of three-dimensional, incompressible, non-chemically reactive, viscous fluids using Fluent software can be described using the Reynolds-averaged equations.

$$\frac{\partial}{\partial t}(\rho k)+\frac{\partial}{\partial x_i}(\rho k u_i)=\frac{\partial}{\partial x_j}(\alpha_k \mu_{eff}\frac{\partial k}{\partial x_j})+G_k+G_b-\rho\varepsilon-Y_M+S_k \quad (1)$$

$$\frac{\partial}{\partial t}(\rho \varepsilon)+\frac{\partial}{\partial x_i}(\rho \varepsilon u_i)=\frac{\partial}{\partial x_j}(\alpha_\varepsilon \mu_{eff}\frac{\partial \varepsilon}{\partial x_j})+C_{1\varepsilon}\frac{\varepsilon}{k}(G_k+C_{3\varepsilon}G_b)-C_{2\varepsilon}\rho\frac{\varepsilon^2}{k}-R_\varepsilon+S_\varepsilon \quad (2)$$

In the equation: ρ represents the fluid density, $C_{1\varepsilon}$=1.42, $C_{2\varepsilon}$=1.68, G_k denotes the generation of turbulent kinetic energy caused by the mean velocity gradient; G_b is the turbulent kinetic energy produced by buoyancy; Y_M represents the contribution of fluctuating dilatation in compressible turbulence to the overall dissipation rate; α_k and α_ε are the reciprocals of the effective Prandtl numbers for k and ε, respectively; S_k and S_ε are user-defined source terms.

2.4 Calculation Method: This study only performs calculations for the computational domain of the pump as turbine. In the Turbulence Model Settings dialog box, select the k-epsilon (2 eqn) model, selecting the submodel as RNG. For high Reynolds number flow problems in the near-wall region, the standard wall function (SWF) method is used to avoid directly solving the regions with significant viscous effects. The gravitational acceleration is set to -9.81 m/s²in the Y direction. The boundary conditions for the inlet and outlet are set as pressure inlet (with an inlet pressure of 8 MPa) and velocity inlet. The inlet condition is set to choose clear water at room temperature as the inlet fluid material for the pump as turbine. Considering viscosity effects, the wall surface is set to no-slip with a roughness of 0.5 mm. In the iterative calculations, all variables use the default under-relaxation factors, and the convergence criterion is a residual less than 10^{-3}.Finally, set different inlet flow rates for repeated calculations. When the residuals meet the required criteria and the monitored physical parameters reach a steady state, stop the computation and read the results.

3 Computational results: Turbulent kinetic energy is a physical quantity that describes the intensity of turbulent motion within a fluid, reflecting the vigor of the turbulent fluctuations present in the fluid flow. Figure 2 displays the contours of turbulent kinetic energy on the Y=0 cross-section of the pump as turbine at inlet flow rates of 177.3 m³/h, 197 m³/h, and 275.8 m³/h, respectively.

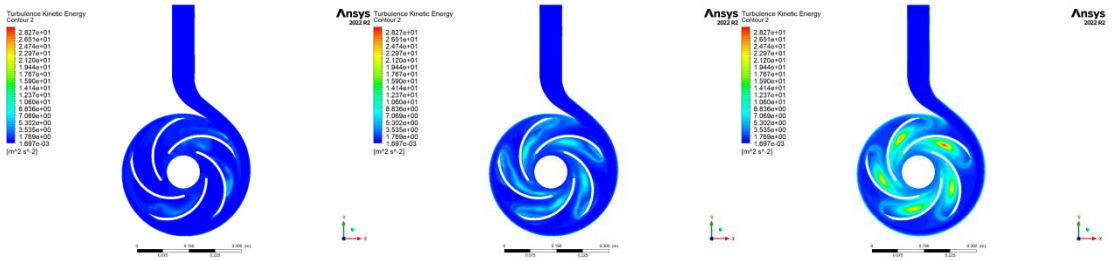

(a) Q=177.3m^3/h **(b) Q=197m^3/hm^3/h** **(c) Q=275.8m^3/h**

Figure 2: Contours of turbulent kinetic energy at different flow rates.

It can be observed that the turbulent kinetic energy is predominantly distributed in the impeller region. The distribution of turbulent kinetic energy decreases as it moves closer to the impeller inlet and outlet. There is almost no distribution of turbulent kinetic energy in the volute and the extended section of the pump as turbine inlet. As the inlet flow rate of the pump as turbine increases, the distribution range and intensity of turbulent kinetic energy in the impeller region gradually expand and strengthen. When the inlet flow rate reaches 275.8 m³/h, the distribution range and intensity of turbulent kinetic energy in the impeller region become significantly large, with the maximum intensity value reaching 28.27 J/kg.

Figure 3 illustrates the vorticity contours on the Y=0 cross-section of the pump functioning as a hydraulic turbine at inlet flow rates of 177.3 m³/h, 197 m³/h, and 275.8 m³/h, respectively. From these three vorticity contour, it can be discerned that when the inlet flow rate is at 177.3 m³/h, there is virtually no distribution of vorticity present. As the inlet flow rate increases, vorticity distribution gradually begins to appear at the trailing edge of the blades, and its extent progressively grows and expands. Additionally, patchy areas of vorticity concentration also start to emerge at the blade roots. When the inlet flow rate reaches 275.8 m³/h, the blades exhibit the maximum vorticity value, which can reach up to 11,570,000 s^{-2}.

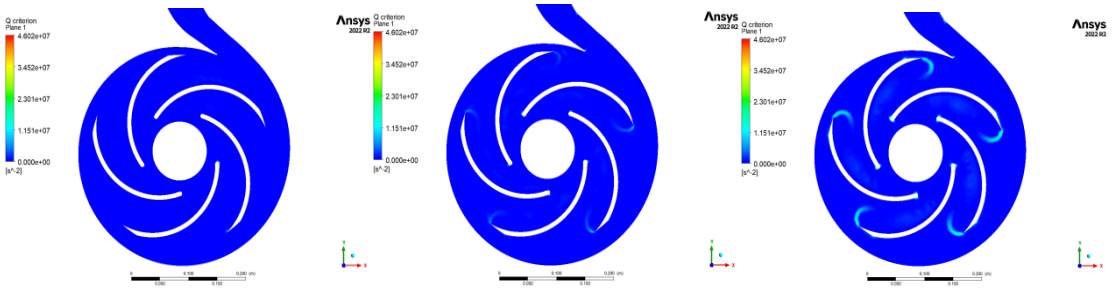

(a) Q=177.3m^3/h **(b) Q=197m^3/hm^3/h** **(c) Q=275.8m^3/h**

Figure 3: Vorticity contours at different flow rates.

To further analyze the internal flow field characteristics of the pump as turbine within the impeller region, Figures 4 and 5 respectively present the pressure and velocity contours on the blade unfolded diagram at inlet flow rates of 177.3 m³/h, 197 m³/h, and 275.8 m³/h.

(a) Q=177.3m^3/h **(b) Q=197m^3/hm^3/h** **(c) Q=275.8m^3/h**

Figure 4: Pressure distribution on the blade unfolded diagram at different flow rates.

(a) Q=177.3m^3/h **(b) Q=197m^3/hm^3/h** **(c) Q=275.8m^3/h**

Figure 5: Velocity distribution on the blade unfolded diagram at different flow rates.

As can be seen from Figure 4, the pressure distribution from the blade inlet to the blade outlet shows a decreasing trend. As the inlet flow rate progressively increases, the overall pressure distribution across the blade unfolded diagram gradually decreases. When the inlet flow rate is 275.8 m³/h, a horseshoe-shaped low-pressure distribution forms at the blade outlet, with the minimum pressure at the center being approximately 1857 kPa. When the inlet flow rate is 177.3 m³/h, the pressure at the blade inlet is relatively high, with the maximum pressure value being approximately 7545 kPa.

As can be seen from Figure 5, the velocity distribution from the blade inlet to the blade outlet exhibits a certain similarity with the pressure distribution, with the flow velocity decreasing as one approaches the blade outlet. When the inlet flow rate is 197 m³/h, a large low-velocity region forms at the blade outlet. However, as the flow rate increases, the extent of this low-velocity region gradually reduces, and the minimum flow velocity can reach 6 m/s. In contrast, as the inlet flow rate increases, the flow velocity at the blade inlet gradually

increases. When the flow rate is 275.8 m³/h, a small high-velocity region appears, with a velocity value reaching up to 96.19 m/s.

To further analyze the flow field characteristics around the blade, Figures 6 and 7 show the streamlines and velocity vector diagrams on the unfolded diagram of the pump as turbine blades, for inlet flow rates of 177.3 m³/h, 197 m³/h, and 275.8 m³/h, respectively.

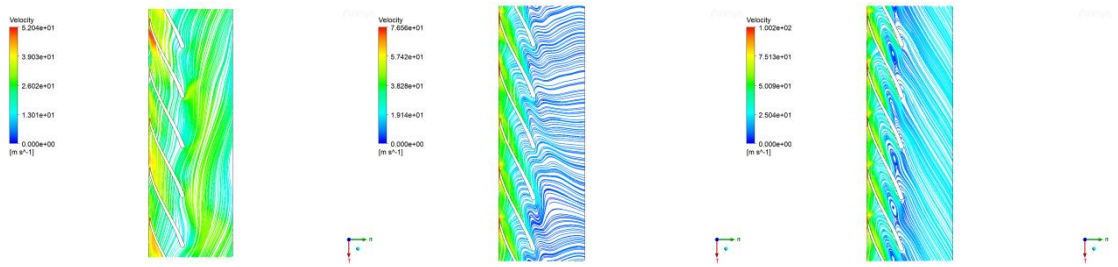

(a) Q=177.3m^3/h **(b) Q=197m^3/hm^3/h** **(c) Q=275.8m^3/h**

Figure 6: Streamline distribution on the blade unfolded diagram at different flow rates.

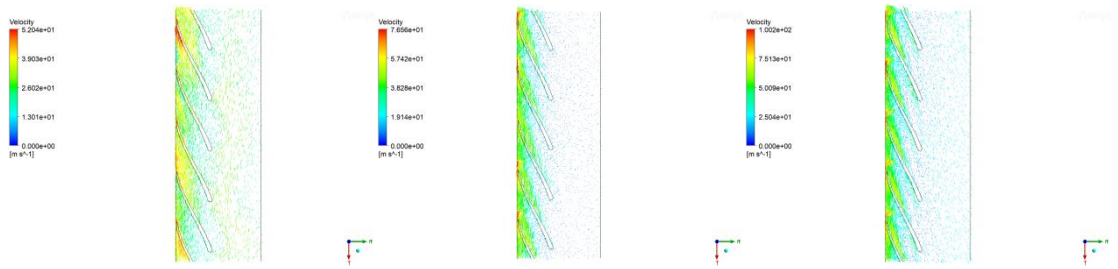

(a) Q=177.3m^3/h **(b) Q=197m^3/hm^3/h** **(c) Q=275.8m^3/h**

Figure 7: Velocity vector distribution on the blade unfolded diagram at different flow rates.

From Figure 6, it can be seen that when the inlet flow rate is 177.3 m³/h, the velocity streamline distribution from the impeller inlet to the impeller outlet is smooth and uniform. As the flow rate increases, the velocity streamlines gradually become distorted and chaotic, especially at the blade outlet. As the flow rate increases, the velocity streamlines gradually become distorted and chaotic, especially at the blade outlet.

As can be seen from Figure 7, as the flow rate increases, the liquid flow direction at the blade outlet gradually deviates from its inherent flow path, resulting in a clockwise deflection flow state. When the inlet flow rate is 275.8 m³/h, a clockwise vortex flow forms at the blade outlet, with slower flow speed and lower density. This bears a certain resemblance to the streamline plots depicted in Figure 6.

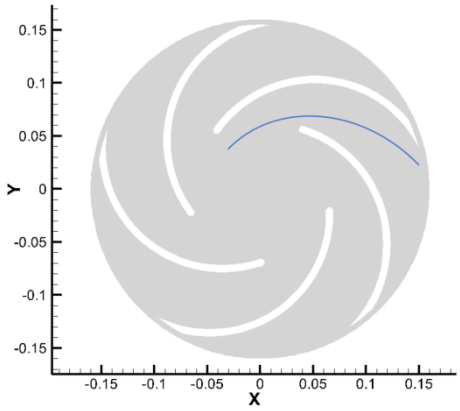

(a) Extraction Line Schematic.

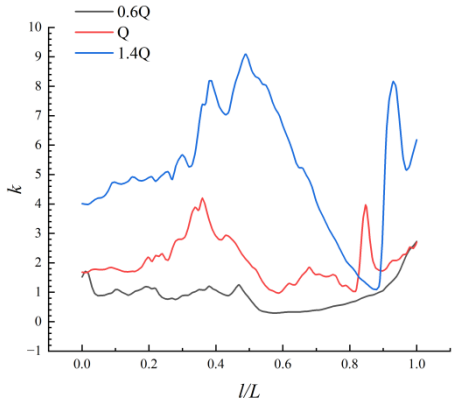

(b) Turbulent kinetic energy variation curve.

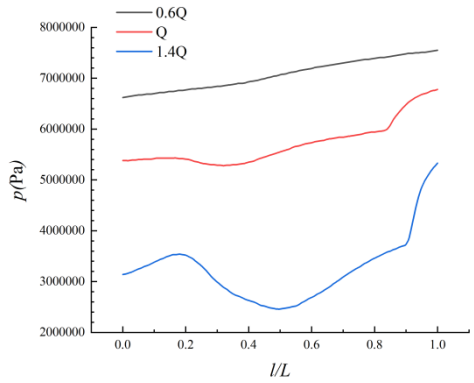

(c) Pressure variation curve.

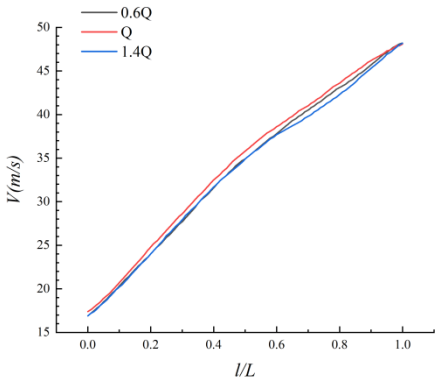

(d) Velocity variation curve.

Figure 8: Variation curves of various physical quantities on the extraction line.

From Figure 8, it can be observed that by extracting a curve from the Y=0 cross-section of the impeller, the variation curves of turbulent kinetic energy, pressure, and velocity from the impeller outlet to the volute section have been calculated. As can be seen from Figure 8(a), the thick blue line in the figure represents the curve extracted from the Y=0 impeller cross-section. In Figures (b), (c), and (d), the abscissa l/L denotes the relative position of the sampling points on the curve, which is the ratio of the distance from the sampling point to the starting point and the length of the curve, with the starting point being at the impeller outlet. As seen in Figure 8(b), there is a sharp increase in turbulence kinetic energy near the impeller edge. With the increase in flow rate, the turbulence kinetic energy at various points along the curve rises to a certain extent. Additionally, the variation patterns of turbulence kinetic energy along the curve at different flow rates show a certain similarity. When the inlet flow rate is 275.8 m^3/h, the highest turbulence kinetic energy of 9.09 J/kg occurs at l/L=0.49 on the curve. From Figure 8(c), it can be observed that the pressure variation curve exhibits a

concave shape. However, as l/L gradually increases, the overall trend of the pressure shows a gradual rise. The bottom range of the concave pressure curve lies between l/L = 0.5 ~ 0.9.As the inlet flow rate decreases, the concave shape of the curve gradually diminishes, and the pressure shows an overall increasing trend. When the flow rate is 275.8 m³/h, the lowest pressure of 2460 kPa occurs at the position l/L=0.5 on the curve. As shown in Figure 8(d), at different flow rates, the velocity gradually increases with the increase in l/L, and the inlet flow rate has little effect on the velocity.

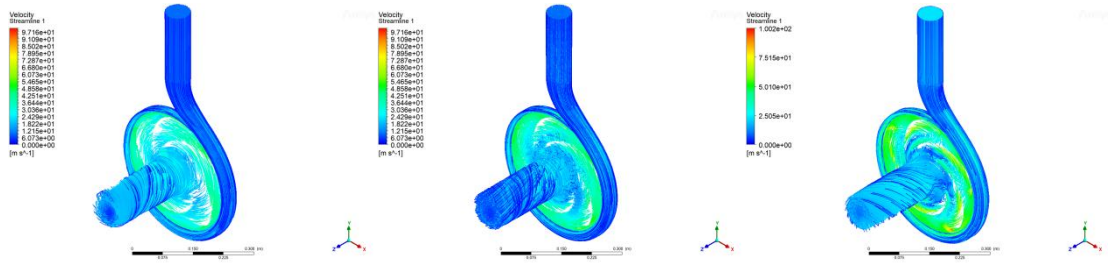

(a) Q=177.3m^3/h **(b) Q=197m^3/hm^3/h** **(c) Q=275.8m^3/h**

Figure 9: Velocity streamlines Chart.

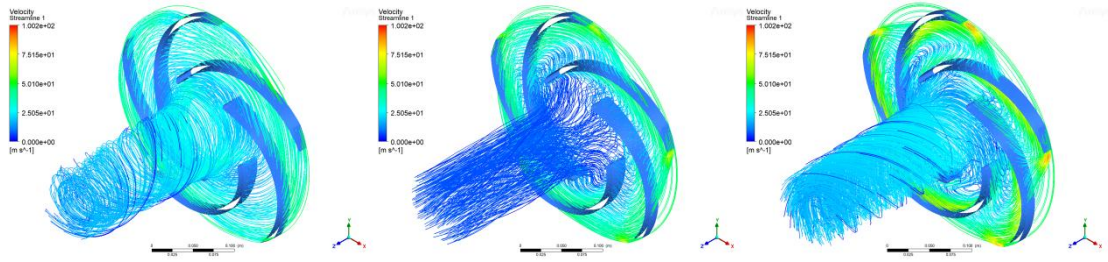

(a) Q=177.3m^3/h **(b) Q=197m^3/hm^3/h** **(c) Q=275.8m^3/h**

Figure 10: Velocity streamlines at the impeller region.

Figures 9 and 10 respectively present the velocity streamline diagrams of the pump as turbine and its impeller section at inlet flow rates of 177.3 m³/h, 197 m³/h, and 275.8 m³/h. From Figure 9, it can be observed that the velocity streamline distribution in the inlet extension and volute section of the pump as turbine is smooth, even, and relatively uniform. From Figure 10, it can be observed that as the flow rate increases, the velocity streamlines at the impeller outlet begin to distort and become chaotic, gradually extending and expanding toward the interior of the impeller. The gas enters the pump as turbine through the inlet and leaves the impeller while rotating. This means that the liquid exits not only with a certain axial velocity, but also with a certain tangential velocity, which makes it rotate and discharge, rather than simply linear. However, when the inlet flow rate is 197 m³/h, the velocity streamlines in the

draft tube become smoother and straighter, with a slower flow velocity. This indicates that the tangential velocity of the liquid within the draft tube decreases during the flow process, and the efficiency of energy conversion by the impeller improves.

4 CONCLUSIONS

As the inlet flow rate increases, the turbulence kinetic energy and vorticity distribution within the pump as turbine significantly increase. The pressure and velocity distribution from the impeller inlet to the impeller outlet both show a gradually decreasing trend. Under high-flow conditions, a horseshoe-shaped low-pressure zone forms at the blade outlet, accompanied by the generation of vortices. On the extraction line at the cross-section Y=0 of the impeller, we extracted the turbulence kinetic energy, pressure, and velocity data. From this, it can be observed that as the flow rate decreases, the turbulent kinetic energy at various parts of the impeller gradually diminishes, and the curve changes tend to become more gradual. As the flow rate increases, a low-pressure zone gradually forms from the middle of the impeller to the impeller inlet. However, along the extraction line, the velocity increases as it approaches the impeller inlet. Different inlet flow rates have little impact on the liquid flow in the inlet extension section of the pump as turbine and within the volute. Under rated operating conditions, the tangential velocity of the fluid in the tail water pipe decreases, the flow rate slows down, and the efficiency of the impeller's energy conversion improves.

ACKNOWLEDGEMENT

The research was financially supported by the national college students science and technology innovation project (No.202411488043).

REFERENCE

1. Tao Wang, Fanyu Kong, Bin Xia, et al. The method for determining blade inlet angle of special impeller using in turbine mode of centrifugal pump as turbine [J]. Renewable Energy, 2017; 109: 518-528.
2. Singh P and Nestmann F. Experimental investigation of the influence of blade height and blade number on the performance of low head axial flow turbines [J]. Renewable Energy, 2011; 36(1): 272-281.
3. Singh P. Optimization of the internal hydraulic and of system design in pumps as turbines with field implementation and evaluation [D]. University of Karlsruhe, Karlsruhe, 2005.

4. Sun-Sheng Yang, Hou-Lin Liu, Fan-Yu Kong, et al. Effects of the Radial Gap Between Impeller Tips and Volute Tongue Influencing the Performance and Pressure Pulsations of Pump as Turbine [J]. Journal of Fluids Engineering, 2014; 136: 054501. 1-8.
5. Yang Junhu, Wang Xiaohui. Effect of vane profile on hydraulic energy recovery turbines performance [J]. Journal of Drainage and Irrigation Machinery Engineering, 2011; 29(4): 287-291.
6. Yang Sunsheng, Kong Fanyu, Shao Fei, Xue Ling,et al.Numerical calculation and experiment of hydraulic turbine [J]. JOURNAL OF JIANGSU UNIVERSITY (Natural Science Edition), 2012; 33(2): 165-169.
7. Fernandez J, Barrio R, Blanco E, et al. Numerical investigation of a centrifugal pump running in reverse mode [J]. Proceedings of the Institution of Mechanical Engineers, Part A: Journal of Power and Energy, 2010; 224(3): 373-381.
8. Jose G., Jesus M. F. O., Katia M. A., et al. Flow analysis for a double suction centrifugal machine in the pump and turbine operation modes [J]. International Journal for Numerical Methods in Fluids, 2009; (61): 220-236.
9. Wang Chunlin, Zeng Cheng, Yang Xiaoyong, Peng Haibo, Liu Dong, et al. Numerical simulation of internal flow field and performance prediction of reversible double suction pump [J]. Journal of Drainage and lrrigation Machinery Engineering, 2015; 33(7): 577-582.
10. Derakhshan S., Nourbakhsh A. Theoretical, numerical and experimental investigation of centrifugal pumps in reverse operation [J]. Experimental Thermal and Fluid Science, 2008; 32(5): 1620-1627.